
Saturation Concentrations of Suspended Fine Sediment. Computations with the Prandtl Mixing-Length Model

C. Kranenburg

Report No. 5 - 98

Prepared for the European Commission, DG XII
MAST3 - COSINUS Project
Contract No. MAS3-CT97-0082

1998

**Saturation Concentrations of Suspended
Fine Sediment. Computations with the
Prandtl Mixing-Length Model**

C. Kranenburg

Report No. 5 - 98

Prepared for the European Commission, DG XII
MAST3 - COSINUS Project
Contract No. MAS3-CT97-0082

1998

Delft University of Technology
Faculty of Civil Engineering and Geosciences
Hydromechanics Section

Abstract

Adopting a 1DV numerical model including the standard $k-\epsilon$ turbulence model, Winterwerp et al. (1999) calculated a saturation concentration for an initially uniform distribution of fine-sediment concentration in steady flow. At concentrations exceeding the saturation concentration the concentration profile collapsed and all sediment was deposited as fluid mud. In this report similar computations are presented using the Prandtl mixing-length model. New expressions for the damping functions accounting for buoyancy effects are derived from three conditions: 1) in the case of equilibrium the concentration should be bounded for all gradient Richardson numbers, 2) the mathematical model should be stable and 3) the relationship between flux Richardson number and gradient Richardson number should agree with empirical data. Numerical results obtained with this model, such as the saturation concentration, agree fairly well with those of Winterwerp et al. (1999). It is shown that the saturation concentration is sensitive to the coefficients in the damping functions. This concentration may increase markedly for values of these coefficients that differ from those selected herein.

Contents

Abstract

1 Introduction

2 1DV Prandtl mixing-length model

2.1 Equations

2.2 Equilibrium distribution

2.3 Damping functions in the PML model

3 Numerical computations

3.1 Case examined

3.2 Results

4 Conclusions

Acknowledgements

References

Figures

1 Introduction

Turbulence tends to counteract the settling of suspended sediment particles, as it causes an upward transport of mass in the case where the sediment concentration increases with depth. In a steady-state situation an equilibrium concentration distribution may exist so that the net vertical transport of sediment vanishes. Teisson et al. (1993) present an argument based on the concept of a maximum flux Richardson number, by which an upper bound to the maximum equilibrium concentration is obtained. Teisson et al. also present results of computations using a Reynolds stress turbulence model that support their argument. Winterwerp et al. (1999) apply the standard k - ϵ turbulence model including buoyancy effects to quasi-uniform flow over a horizontal bed and the vertical exchange of fine sediment. Initially the vertical concentration distribution is uniform and the velocity distribution is logarithmic. Those authors find that in steady flow a complete collapse of the concentration profile will result, if the initial concentration exceeds a critical value and the deposited sediment behaves as a dense fluid (fluid mud). This critical value is denoted herein as the saturation concentration.

A turbulence model that is easy to implement is the Prandtl mixing-length (PML) model. In this model density stratification caused by the sediment is accounted for by so-called damping functions which depend on the gradient Richardson number. These functions are derived from observations in most cases, and therefore lack universality. As a consequence, the simplicity of the PML model is at the expense of a less predictive value for sediment-laden flow.

The purpose of this report is to derive conditions the damping functions have to satisfy, so that the PML model is in agreement with the analysis of Teisson et al. (1993) and, as a consequence, also predicts a saturation concentration. These conditions aid in estimating damping functions from empirical data.

The determination of the damping functions indicated is presented in Section 2 of this report. Results of numerical simulations similar to those of Winterwerp et al. (1999) are discussed in Section 3. Conclusions resulting from this work are drawn in Section 4.

2 1DV Prandtl mixing-length model

2.1 Equations

The flow considered is quasi-uniform, shallow-water shear flow over a horizontal bed. Fine sediment is suspended in this flow.

Neglecting advective acceleration and adopting the Boussinesq approximation, the equation of motion in the direction of the flow becomes

$$\frac{\partial U}{\partial t} = -g \frac{\partial h}{\partial x} - \frac{\partial}{\partial z} \langle uw \rangle \quad (2.1)$$

where U is the mean flow velocity, t time, g the acceleration of gravity, h the water depth, x the streamwise coordinate, z the vertical coordinate (positive upward, $z = 0$ at the bed) and $\langle uw \rangle$ the turbulent shear stress.

Imposing a discharge q given by

$$q = \int_0^h U dz \quad (2.2)$$

that does not change with time and assuming zero shear stress at the free surface, (2.1) can be written as

$$\frac{\partial U}{\partial t} = \frac{u_*^2}{h} - \frac{\partial}{\partial z} \langle uw \rangle \quad (2.3)$$

where u_* is the (time dependent) friction velocity at the bed given by $u_*^2 = -\langle uw \rangle(z_0, t)$. Here z_0 is the roughness height of the bed, which is assumed hydraulically rough.

The 1DV mass balance equation for the sediment reads

$$\frac{\partial C}{\partial t} = \frac{\partial}{\partial z} (W_s C - \langle wc \rangle) \quad (2.4)$$

where C is the mean concentration, W_s the settling velocity and $\langle wc \rangle$ the vertical turbulent mass transport. The effect of hindered settling on the settling velocity is not considered herein, because it is not needed for the analysis. However, it could be included easily.

The equations for turbulence closure according to the PML model can be written as (e.g., Rodi, 1980)

$$\langle uw \rangle = -l^2(z) \left| \frac{\partial U}{\partial z} \right| \frac{\partial U}{\partial z} F(Ri) \quad (2.5)$$

$$\langle wc \rangle = -\frac{l^2(z)}{\sigma_t} \left| \frac{\partial U}{\partial z} \right| \frac{\partial C}{\partial z} G(Ri) \quad (2.6)$$

where $l(z)$ and σ_t are mixing length and turbulent Prandtl-Schmidt number under neutral conditions, F and G are damping functions, and Ri is the gradient Richardson number defined by

$$Ri = -\frac{\Delta g}{\rho_w} \frac{\partial C}{\partial z} \left(\frac{\partial U}{\partial z} \right)^{-2} \quad (2.7)$$

Here $\Delta = (\rho_s - \rho_w)/\rho_s$, ρ_s is the density of the sediment and ρ_w the density of the water.

The assumed distribution of the mixing length in the water column is the Bakhmetev profile,

$$l(z) = \kappa z \left(1 - \frac{z}{h} \right)^{1/2} \quad (2.8)$$

where $\kappa \approx 0.41$ is the Von Karman constant.

The boundary conditions at the free surface are

$$\langle uw \rangle(h,t) = 0 \quad (2.9)$$

$$W_s C(h,t) - \langle wc \rangle(h,t) = 0 \quad (2.10)$$

Equations (2.9) and (2.5) yield as a condition for the velocity that $\partial^2 U(h,t)/\partial z^2$ should vanish. Equations (2.10) and (2.6) give $C(h,t) = 0$. The boundary conditions at the bed are

$$U(z_0,t) = 0 \quad (2.11)$$

$$W_s C(z_0,t) - \langle wc \rangle(z_0,t) = 0 \quad (2.12)$$

Assuming near-neutral conditions near the bed, the above equations yield for the Richardson number at $z = z_0$

$$Ri(z_0, t) \approx \kappa \sigma_t \frac{\Delta g W_s z_0}{u_*^3} \frac{C(z_0, t)}{\rho_w} \quad (2.13)$$

The conditions near the bed are indeed near-neutral provided $Ri(z_0, t) \ll 1$. This condition is satisfied for fine sediments in many cases, unless the sediment is deposited.

Deposited sediment is treated as fluid mud, that is, as a dense fluid.

2.2 Equilibrium conditions

An equilibrium concentration distribution may develop under steady-state conditions. The time derivatives in (2.3) and (2.4) then vanish so that these equations together with (2.5) - (2.8) give

$$\frac{Ri G(Ri)}{\sigma_t F^{3/2}(Ri)} = \kappa \frac{\Delta g W_s h}{u_*^3} \frac{z}{h - z} \frac{C(z)}{\rho_w} \quad (2.14)$$

The right-hand side of this equation is identical to Teisson et al.'s (1993) estimate of the flux Richardson number in the case of equilibrium. Because in shear flow the flux Richardson number is bounded (also see Section 2.3), this implies for the PML model that the left-hand side of (2.14) also should be bounded. Defining damping functions F and G in the interval $0 \leq Ri < \infty$, this means that the left-hand side of (2.14) should be bounded for all $Ri \geq 0$. This condition will always be satisfied, if the limit of $RiG/F^{3/2}$ for $Ri \rightarrow \infty$ exists.

Assuming damping functions of the well-known form

$$F(Ri) = (1 + A Ri)^{-a} \quad (2.15)$$

$$G(Ri) = (1 + B Ri)^{-b} \quad (2.16)$$

where A , B , a and b are positive constants, it is therefore required that

$$1 + \frac{3}{2}a - b \leq 0 \quad (2.17)$$

Kranenburg (1982) derived stability conditions for the mathematical model under consideration (that is, not a discretised representation of it) by requiring that small-amplitude disturbances superimposed on a steady-state solution do not grow. In the case of (2.15) and (2.16), a sufficient condition for stability resulting from this work is

$$1 + \frac{3}{2}a - b \geq 0 \quad (2.18)$$

The PML model therefore satisfies both Teisson et al.'s (1993) result and the stability condition (2.18), provided

$$1 + \frac{3}{2}a - b = 0 \quad (2.19)$$

2.3 Damping functions in the PML model

Damping functions are not only used in the PML model, but also in turbulence models of the Taylor-Kolmogorov (TK) type. In 1DV models of the latter type (minus) the vertical velocity and concentration gradients are multiplied by an algebraic eddy viscosity and eddy diffusivity, respectively, to obtain vertical turbulent transports of momentum and mass. The damping functions in these two types of models are different, as can be seen in the following way.

Denoting damping functions in the PML model by F_P and G_P , and those in the TK model by F_{TK} and G_{TK} , the two turbulence models can be written, for $\partial U/\partial z > 0$, as

$$\langle uw \rangle = -l^2 \left(\frac{\partial U}{\partial z} \right)^2 F_P = -u_* l \frac{\partial U}{\partial z} F_{TK} \quad (2.20)$$

$$\langle wc \rangle = -\frac{l^2}{\sigma_t} \frac{\partial U}{\partial z} \frac{\partial C}{\partial z} G_P = -\frac{u_* l}{\sigma_t} \frac{\partial C}{\partial z} G_{TK} \quad (2.21)$$

Assuming in these equations $\langle uw \rangle = -u_*^2$, it follows that

$$F_P = F_{TK}^2 \quad (2.22)$$

$$G_P = F_{TK} G_{TK} \quad (2.23)$$

These results satisfy the condition that all damping functions are equal to one for $Ri = 0$. Furthermore, the expression for the turbulent Prandtl-Schmidt number ($=\sigma_t F/G$) is the same for both models: $\sigma_t F_P/G_P = \sigma_t F_{TK}/G_{TK}$.

The widely used Munk-Anderson (1948) damping functions, for example, apply to the TK model and have, in (2.15) and (2.16), $a = 0.5$ and $b = 1.5$. Substituting from (2.22) and (2.23) and assuming for the sake of convenience $B = A$, the corresponding damping functions in the PML model have $a = 2 \times 0.5 = 1.0$ and $b = 0.5 + 1.5 = 2.0$. It is noted that these values of a and b do not satisfy (2.19).

Further quantitative results for the damping functions can be obtained from empirical data concerning the flux Richardson number R_f , which for the PML model becomes

$$R_f = \frac{\Delta g \langle wc \rangle}{-\rho_w \langle uw \rangle \partial U / \partial z} = \frac{Ri G_P}{\sigma_t F_P} \quad (2.24)$$

Again assuming $B = A$ and adopting (2.19), R_f is found to reach a maximum for $Ri = Ri_m = 2/(aA)$. The maximum, R_{fm} , of R_f is given by

$$R_{fm} = \frac{Ri_m}{\sigma_t} \left(\frac{a}{2 + a} \right)^{(2 + a)/2} \quad (2.25)$$

Reasonable values of R_{fm} and Ri_m are about 0.15 and 0.4, respectively (e.g., Schumann and Gerz, 1995; Mizushima et al. 1978). Assuming $\sigma_t = 0.7$ this gives $A = B = 2.4$ and $a = 2$ (so that $b = 4$).

Taking into account (2.22) and (2.23), the damping functions thus obtained agree fairly well with the data of Ueda et al. (1981). However, these functions underestimate the damping found by Uittenbogaard (1993). Lehfeldt and Bloss (1988) applied (2.15) and (2.16) with $A = B = 3$ and $a = 1$, $b = 3$ together with the TK model. These values of a and b correspond with those obtained for the PML model. Lehfeldt and Bloss found satisfactory agreement with observations of salinity and temperature in a well-mixed estuary and in a stratified estuary.

In the case where $B = A$ and (2.19) is satisfied, it follows from (2.14) that for an equilibrium distribution

$$\frac{C(z)}{\rho_w} < \frac{1}{\kappa \sigma_t A} \frac{u_*^3}{\Delta g W_s h} \frac{h - z}{z} \quad (2.26)$$

This result is similar to that derived by Teisson et al. (1993). As a numerical example the case examined by Winterwerp et al. (1999) is considered:

$$\rho_w = 1020 \text{ kg/m}^3,$$

$$\rho_s = 2650 \text{ kg/m}^3,$$

$$\kappa = 0.41,$$

$$\sigma_t = 0.7,$$

$$h = 16 \text{ m},$$

$$W_s = 0.5 \text{ mm/s and}$$

$u_* = 9.45 \text{ mm/s}$ (which is the initial value in the computations of these authors, who assumed $z_0 = 1 \text{ mm}$ and depth-averaged flow velocity = 0.2 m/s).

Furthermore, $A = 2.4$. For these values of the parameters, (2.26) gives for the concentration at mid-depth, for example: $C(h/2) < 0.026 \text{ kg/m}^3$. This upper bound is close to the saturation concentration of 0.023 kg/m^3 found by Winterwerp et al. (1999).

3 Numerical computations

3.1 Case examined

To compare results of the PML model with results of the standard k- ϵ model (Winterwerp et al., 1999) in greater detail, Equations (2.3) - (2.12) were solved numerically for the conditions those authors selected.

As before, the water depth is 16 m, the roughness height is 1 mm, the depth-averaged flow velocity is constant and equal to 0.2 m/s, the settling velocity is 0.5 mm/s, the densities of water and sediment are 1020 and 2650 kg/m³, the turbulent Prandtl-Schmidt number for neutral conditions is 0.7, and the Von Karman constant is 0.41. The coefficients in the damping functions are adopted from the previous section: A = B = 2.4, a = 2 and b = 4.

The numerical scheme used is the explicit Euler scheme, the time step is 1 s, and the water column is discretised in 51 equidistant grid points. The differences from computations with 101 grid points are minor.

A logarithmic velocity profile and a uniform concentration distribution are prescribed as initial conditions,

$$U(z,0) = \frac{u_*}{\kappa} \ln \frac{z}{z_0} \quad (3.1)$$

$$C(z,0) = C_i \quad (3.2)$$

where C_i is a constant.

The boundary conditions are given by (2.9) - (2.12). The friction velocity u_* , which decreases in the course of time because of density stratification, is determined from an approximate analytical solution near the bed of (2.5) in which $\langle uw \rangle \approx -u_*^2$, (2.8) in which $z/h \ll 1$, and (2.15) in which use is made of the computed value of Ri in the first grid point above the bed. Stratification is included, because in the case of collapse of the concentration profile the flow near the bed becomes stratified.

3.2 Results

Some computational results are shown in Figures 3.1, 3.2 and 3.3 for $C_i = 0.010$, 0.020 and 0.024 kg/m³, respectively. Figure 3.1 shows that in an upper part of the water column the sediment initially settles, as a result of which concentrations closer to the bed increase. Equilibrium is reached relatively fast, after about 400 min. The velocity distribution hardly changes with time. At the higher initial concentration of 0.020 kg/m³ the concentrations near the bed become much higher and much more time is needed to reach equilibrium (about 900 min., see Figure 3.2).

Figure 3.3 with $C_i = 0.024$ kg/m³ shows a completely different picture. Although a tendency to develop an equilibrium concentration distribution exists during the first 500 min. or so, the

concentration profile eventually collapses completely so that after about 1000 min. all sediment has deposited. The time needed for collapse is about twice the time scale for settling, h/W_s . Again the velocities are much less affected. The decreasing velocity at the lutocline near the bed implies a decreasing bed shear stress.

Apparently, a critical initial concentration exists beyond which the concentration distribution becomes supersaturated so that all sediment is deposited. This result agrees quite well with that of Winterwerp et al. (1999). As stated before, those authors found a saturation concentration of 0.023 kg/m^3 . For $C_i = 0.024 \text{ kg/m}^3$ Winterwerp et al. found complete collapse of the concentration profile after about 1250 min.

In the present calculations a partial collapse occurs for $0.021 \leq C_i \leq 0.023 \text{ kg/m}^3$. An example is shown in Figure 3.4 for $C_i = 0.022 \text{ kg/m}^3$. The more gradual transition from subsaturated to supersaturated conditions in the present results affects the shape of the equilibrium concentration profile. The equilibrium distribution of C/C_i Winterwerp et al. calculate for $C_i = 0.023 \text{ kg/m}^3$, for example, shows more resemblance with the equilibrium profile obtained herein for $C_i = 0.010 \text{ kg/m}^3$ (Figure 3.1) than with that for $C_i = 0.020 \text{ kg/m}^3$ (Figure 3.2).

The sensitivity of the results to the exponents a and b in the damping functions is illustrated in Figures 3.5 and 3.6. Figure 3.5 shows results for $b = 3$ and $C_i = 0.040 \text{ kg/m}^3$, while the remaining parameters remain unchanged. This value of b does not satisfy (2.17), as a result of which a stable equilibrium distribution is obtained for a much higher initial concentration. In this case the range of concentrations for which partial collapse is found, is much wider. Complete collapse occurs for $C_i > 0.064 \text{ kg/m}^3$. Figure 3.6 shows similar results for $a = 3$, also at variance with (2.17), and $C_i = 0.035 \text{ kg/m}^3$. Although the damping of turbulent shear stress is increased in this case, equilibrium is again found for much higher initial concentrations.

The sensitivity to the coefficients A and B is also considerable, though to a lesser extent than that to a and b . Increasing A and B to 3, for example, reduces the saturation concentration to 0.016 kg/m^3 .

4 Conclusions

The damping functions that result from this work were derived from three conditions: 1) in the case of equilibrium the concentration should be bounded for all gradient Richardson numbers, 2) the mathematical model should be stable, and 3) the relationship between flux Richardson number and gradient Richardson numbers should agree with empirical data. The damping functions obtained show a stronger damping for increasing gradient Richardson number, Ri , than those usually adopted in the literature. A partial explanation for this fact is the often overlooked difference of damping functions for the PML model from those for the TK model, as indicated by (2.22) and (2.23). These equations imply a stronger damping for large Ri in the functions for the PML model.

With the damping functions derived, the numerically predicted saturation concentration agrees well with that obtained by Winterwerp et al. (1999) using the standard $k-\epsilon$ model. The times needed for the deposition of all sediment under supersaturated conditions are comparable for both models. This agreement may be somewhat fortuitous because of the differences in turbulence modelling and the high sensitivity of the present results to changes in the coefficients in the damping functions. As opposed to the $k-\epsilon$ model, the PML model predicts a certain range of initial concentrations for which partial collapse of the concentration profile occurs. Although this range is small, differences in the shape of the equilibrium concentration profile exist for a much wider range of initial concentrations.

As damping functions lack universality, different values of the coefficients in these functions may be required for other types of flow and turbulent exchange. In this respect the $k-\epsilon$ model is more generally applicable. This report therefore is not meant as a recommendation for replacing the $k-\epsilon$ model with the PML model.

Acknowledgements

The author is grateful to Mr A.M. den Toom of the Laboratory of Hydromechanics, who implemented the PML model. This work was carried out as part of the MAST3-COSINUS Project. It was partially funded by the European Commission, Directorate General XII, under Contract No. MAS3-CT97-0082.

References

- Kranenburg, C. (1982) Stability conditions for gradient-transport models of turbulent density-stratified flow. *Geophys. Astrophys. Fluid Dynamics* **19**, pp. 93-104.
- Lehfeldt, R. and S. Bloss (1988) Algebraic turbulence model for stratified tidal flows. In: *Physical Processes in Estuaries* (J. Dronkers and W. van Leussen, Eds.). Springer-Verlag, Berlin, pp. 278-291.
- Mizushima, T., F. Ogino, H. Ueda and S. Komori (1978) Buoyancy effect on diffusivities in thermally stratified flow in open channel. In: *Heat transfer 1978* **1**. Hemisphere, Washington DC, pp. 91-96.
- Munk, W.H. and E.R. Andersen (1948) Notes on a theory of the thermocline. *J. Marine Res.* **VII**, pp. 276-295.
- Rodi, W. (1980) *Turbulence Models and their Application in Hydraulics*. International Association for Hydraulic Research, Delft, The Netherlands.
- Schumann, U. and T. Gerz (1995) Turbulent mixing in stably stratified shear flows. *J. Appl. Meteorol.* **34**, pp. 33-48.
- Teisson, Ch., O. Simonin, J.C. Galland and D. Laurence (1993) Turbulence and mud sedimentation: A Reynolds stress model and a two-phase flow model. In: *Proc. 23rd Int. Conf. on Coastal Engineering* (B.L. Edge, Ed.) **3**, pp. 2853-2866.
- Ueda, H., S. Mitsumoto and S. Komori (1981) Buoyancy effects on the turbulent transport processes in the lower atmosphere. *Quart. J. R. Met. Soc.* **107**, pp. 561-578.
- Uittenbogaard, R.E. (1993) Testing some damping functions for mixing-length turbulence models. *Report Z721*. Delft Hydraulics.
- Winterwerp, J.C., R.E. Uittenbogaard and J.M. de Kok (1999) Rapid siltation from saturated mud suspensions. Submitted to: *Proc. 5th Int. Conf. on Cohesive Sediment Transport, INTERCOH'98*.

FIGURES

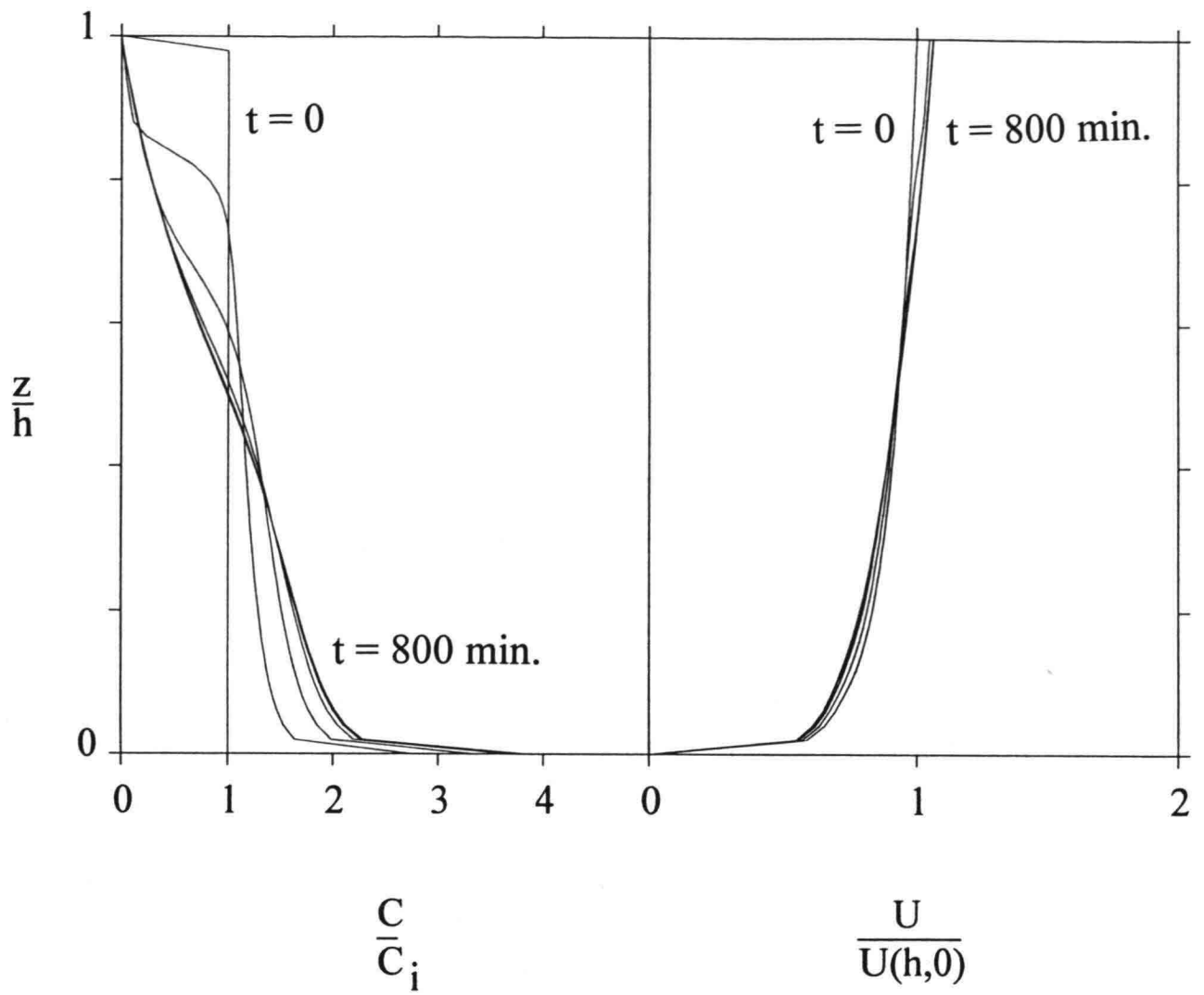


Figure 3.1. Concentration and velocity distributions for $C_i = 0.010 \text{ kg/m}^3$. Time interval between plots is 100 min. Total simulation time is 800 min.

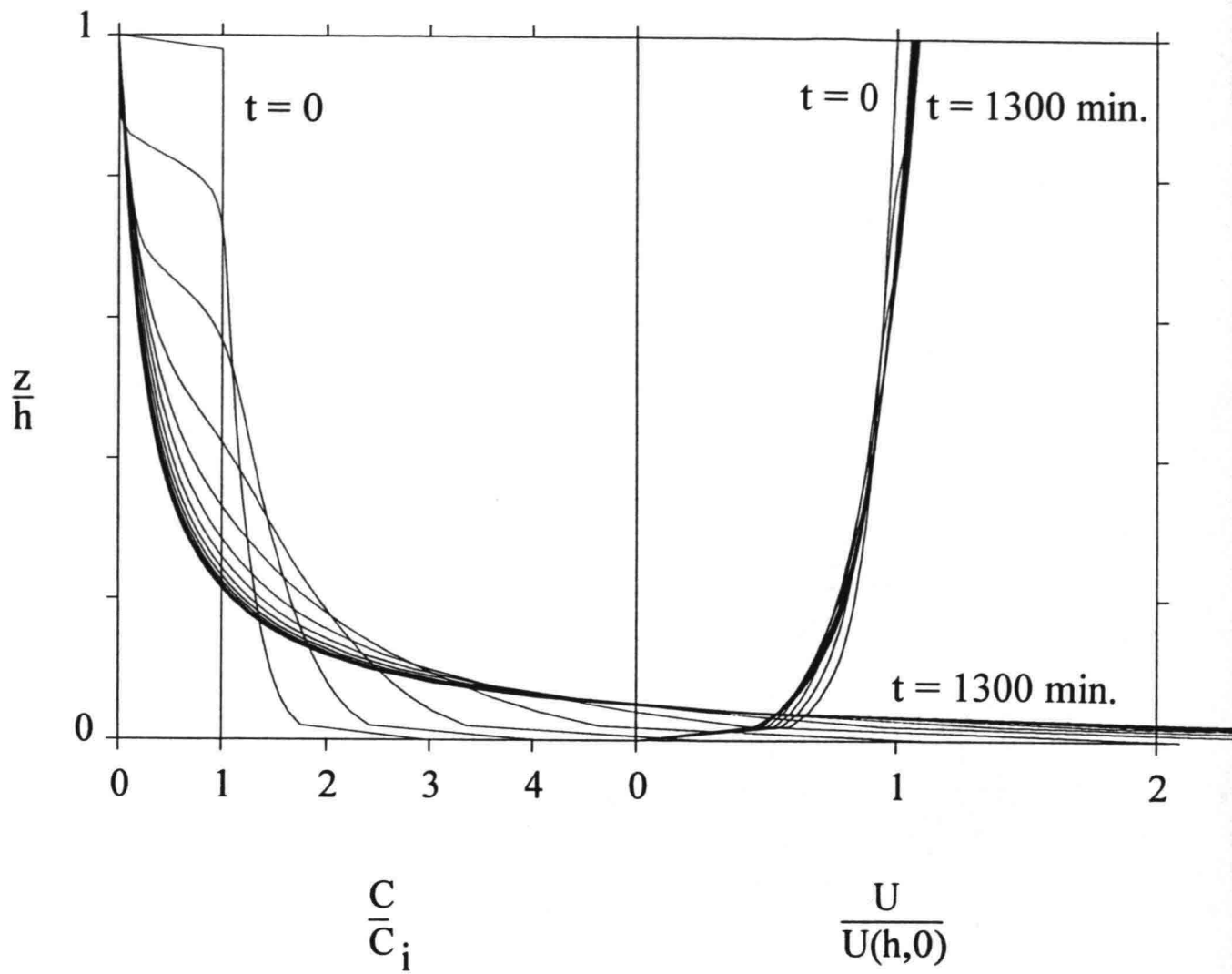


Figure 3.2. Concentration and velocity distributions for $C_i = 0.020 \text{ kg/m}^3$. Time interval between plots is 100 min. Total simulation time is 1300 min.

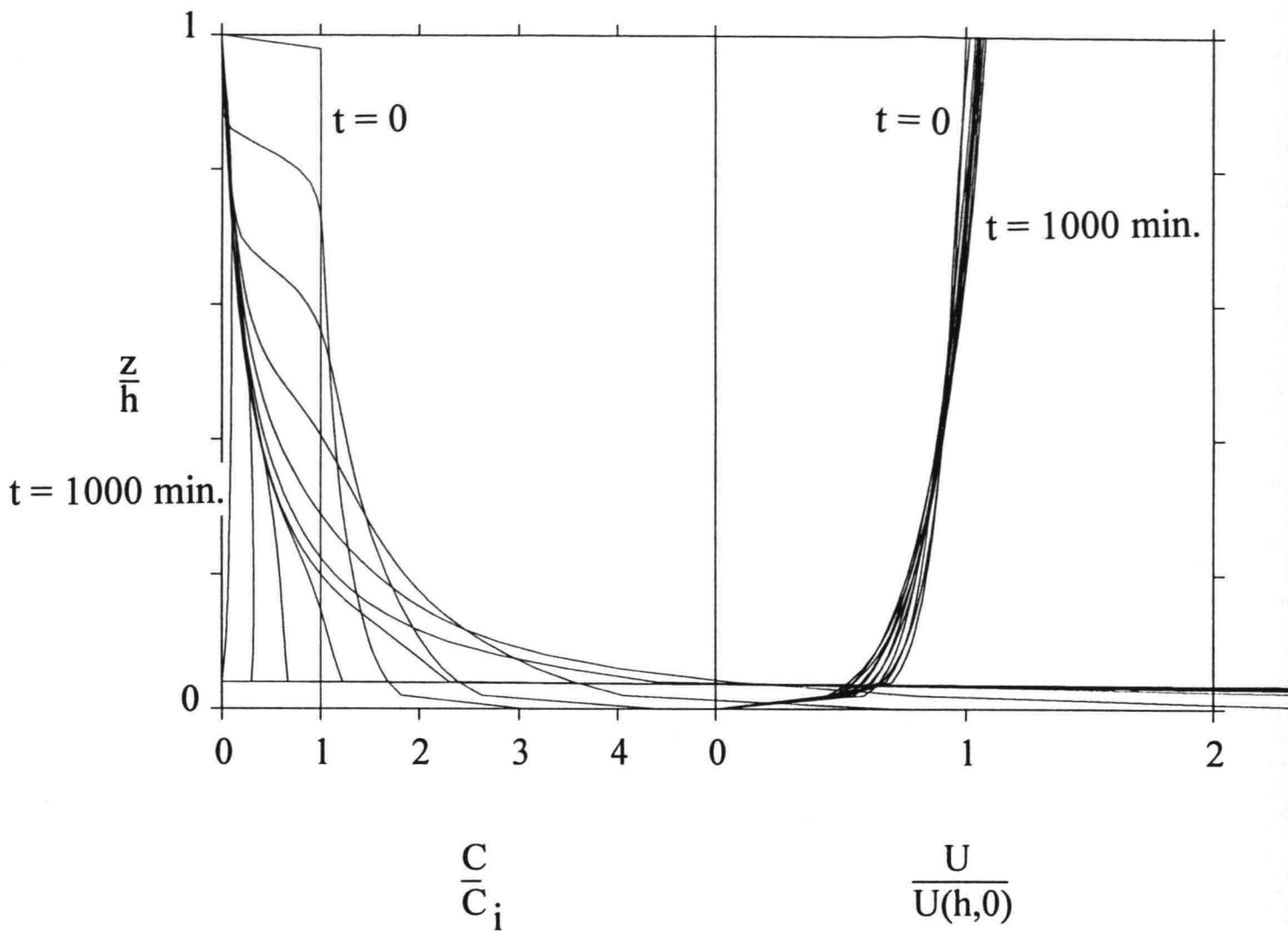


Figure 3.3. Concentration and velocity distributions for $C_i = 0.024 \text{ kg/m}^3$. Time interval between plots is 100 min. Total simulation time is 1000 min.

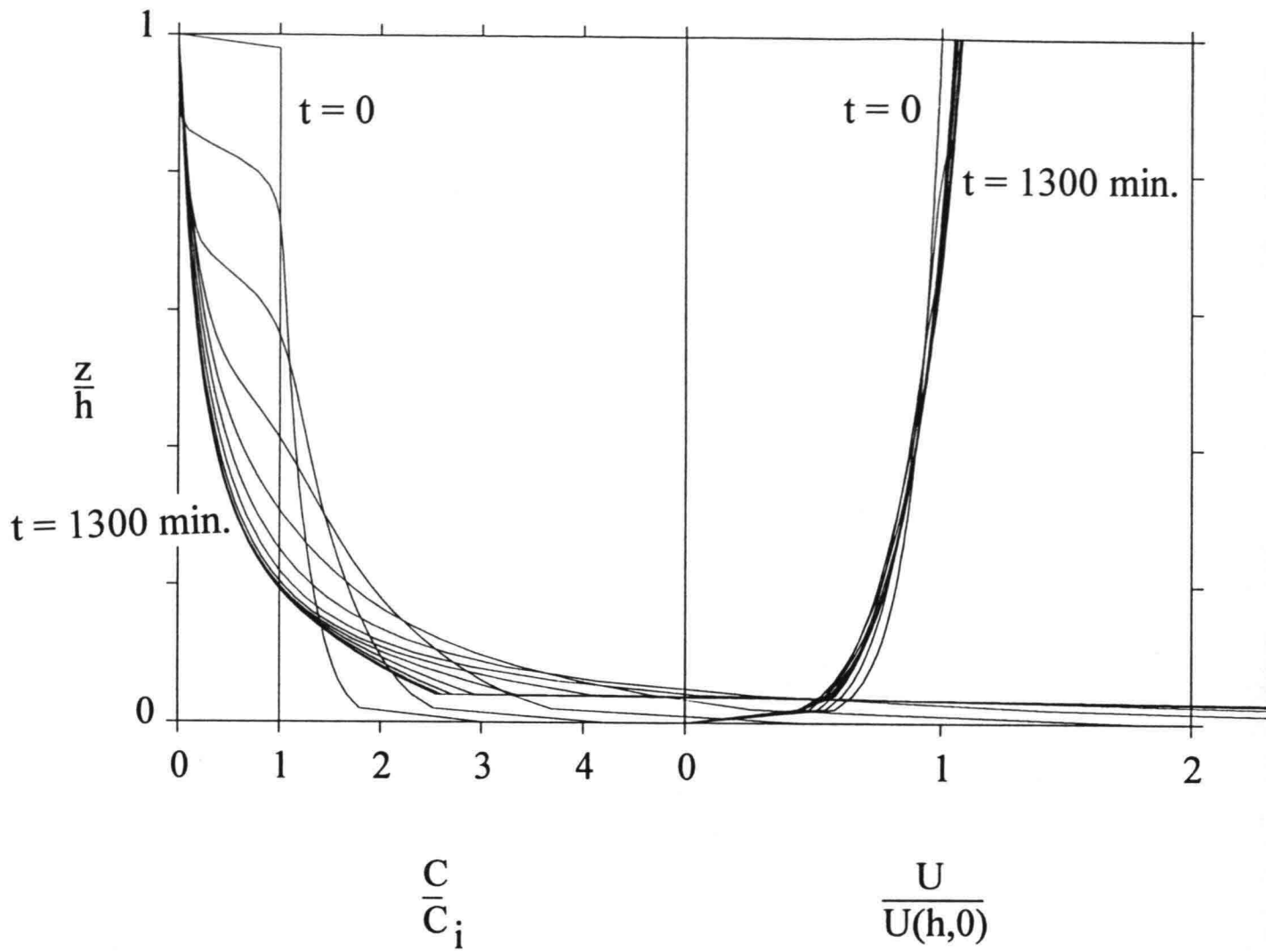


Figure 3.4. Concentration and velocity distributions for $C_i = 0.022 \text{ kg/m}^3$. Time interval between plots is 100 min. Total simulation time is 1300 min. The kink in the final concentration distribution at $C/C_i \approx 2.6$ indicates partial collapse of the concentration profile.

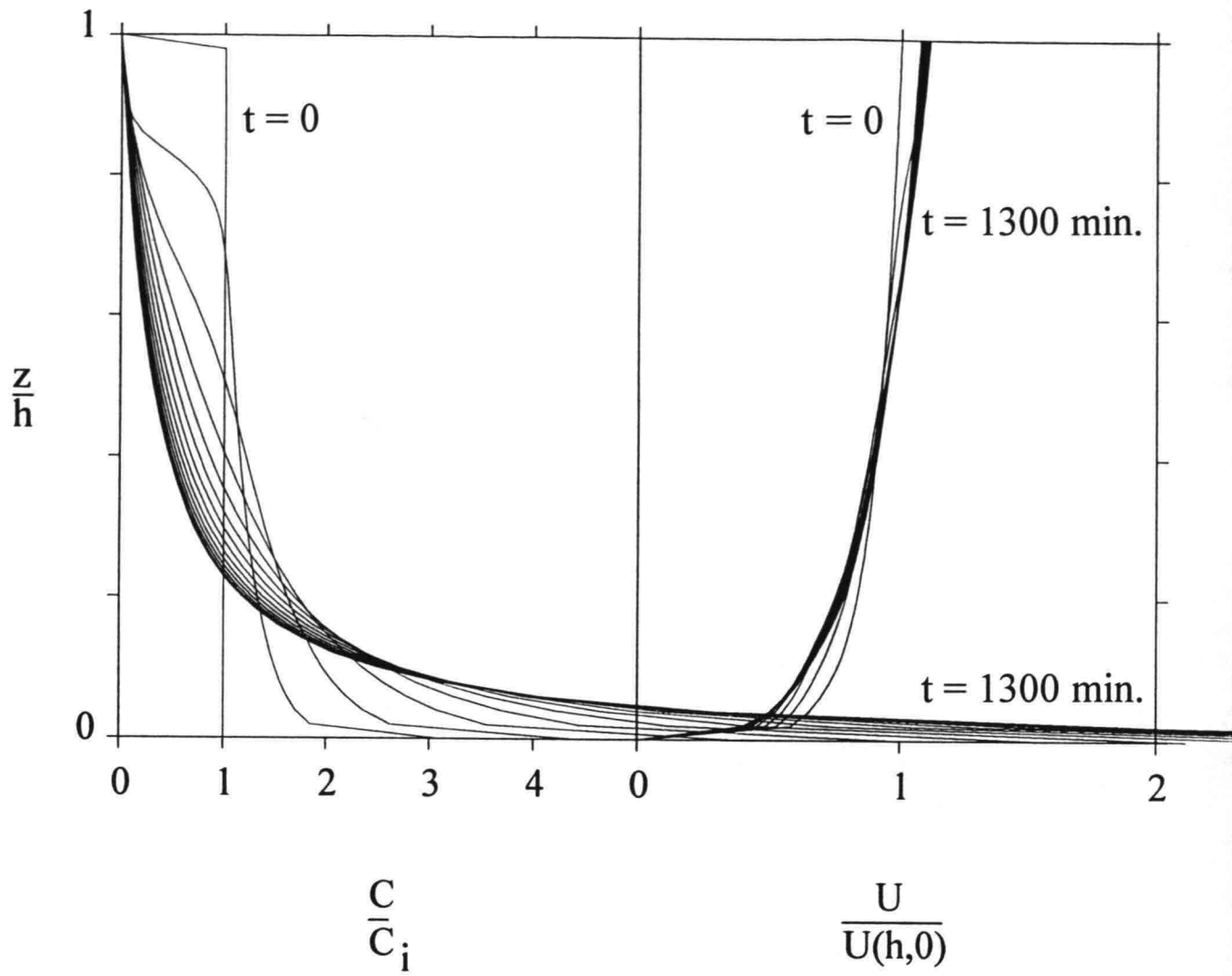


Figure 3.5. Concentration and velocity distributions for $C_i = 0.040 \text{ kg/m}^3$, $a = 2$ and $b = 3$. Time interval between plots is 100 min. Total simulation time is 1300 min.

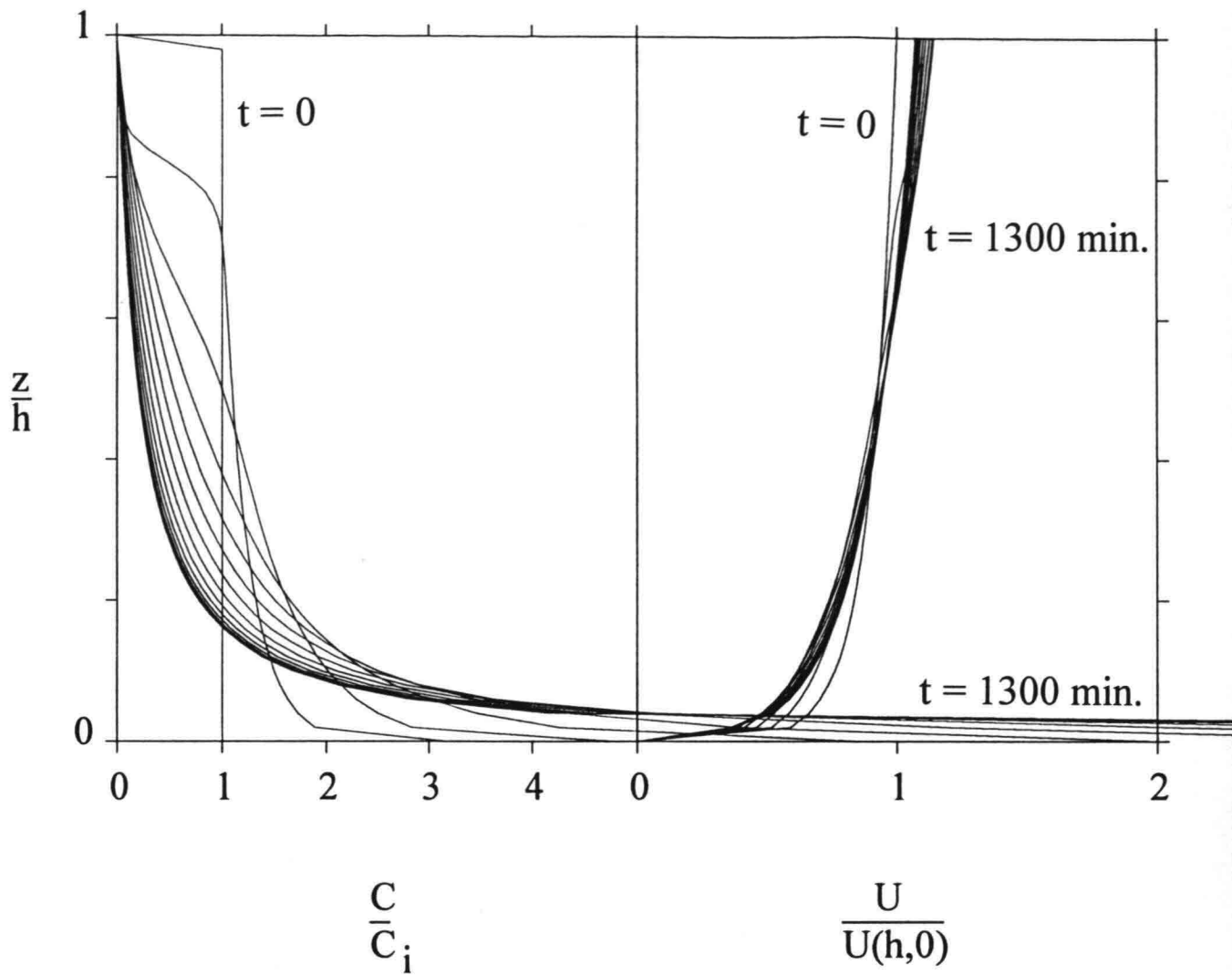


Figure 3.6. Concentration and velocity distributions for $C_i = 0.035 \text{ kg/m}^3$, $a = 3$ and $b = 4$. Time interval between plots is 100 min. Total simulation time is 1300 min.

